5-2021

Cacna1g transcript knockdown analysis via in situ hybridization

Jennifer (Shih-En) Chen

Cacna1g transcript knockdown analysis via *in situ* hybridization

A thesis submitted in partial fulfillment of the requirement
for the degree of Bachelor of Science in Neuroscience from
William & Mary

by

Jennifer (Shih-En) Chen

Accepted for _____
(Honors, High Honors, Highest Honors)

_____
Christopher Del Negro, Ph.D

_____
Jennifer Bestman, Ph.D

_____
Dana Lashley, Ph.D
Randolph Coleman

_____
Randolph Coleman, Ph.D

Williamsburg, VA
May 7, 2021

Acknowledgements

I would first like to thank my principal investigator, Dr. Christopher Del Negro, for giving me the opportunity to learn and conduct research with him since my freshman year. Research with Dr. Del Negro has been a huge part of my undergraduate experience, and I have learned essential skills that can be applied to my future endeavors. During my time in this lab, I am also fortunate to develop a close relationship with Dr. Maria Cristina Picardo, who provided constant encouragement, advice, and mentorship. I would also like to thank Cam Grover for his support, willingness to answer my questions, and patience throughout the years.

I would also like to thank my committee members, Dr. Jennifer Bestman, Dr. Dana Lashley, and Dr. Randolph Coleman. Thank you Dr. Bestman, for two great semesters of neuroscience classes where we had the opportunity to geek out over neuroscience and Korean dishes. Thank you, Dr. Lashley, for making organic chemistry interesting. The rigor and challenge of the class excited me to study and help out fellow students. Thank you Dr. Coleman, for the course advice and encouraging my pursuit of a medical career.

I am also very blessed with numerous friends who encourage me, listen to my complaints, and never stopped believing in me. Thank you Wei Qian Lim, for being the sister I never had and always being an MVP in giving advice. Thank you to all my housemates, Gabi Cao, Andrea Hooberman-Pineiro, Margot Szamosszegi, and Chloe Trinh, for providing me comfort and laughs when I need it. Thank you Erica Ahl, for being an invaluable presence and a constant source of positive energy.

Lastly, I would like to thank my family and God, who are my pillars especially during these uncertain times. I am truly and forever grateful to everyone.

Table of Contents

Abstract

The pedunculopontine nucleus (PPN) comprises the mesencephalic locomotor region (MLR) of the midbrain. It contains glutamatergic, cholinergic, and GABAergic interneurons, but only glutamatergic neurons influence locomotion, which is our focus here. The PPN receives upstream and downstream input from the basal ganglia. It projects to the reticular formation of the brainstem, which connects to the spinal cord. The PPN is involved in a wide range of physiological and behavioral processes, but our focus is locomotion. We hypothesize that the PPN influences the reticular activating system (RAS) of the medulla and thus the central pattern generators (CPG) in the spinal cord via CaV3.1 proteins, which are voltage gated low-threshold Ca^{2+} channels. We contend that CaV3.1 proteins are evoked by disinhibition and mediate burst responses that cause downstream postsynaptic activation of the RAS and ultimately the CPG in the spinal cord. To test this idea, this study aims to study the down regulation of CaV3.1 proteins by the knockdown of its underlying gene, *Cacna1g* via shRNA payloads during viral vector delivery. We employed multiplex *in situ* hybridization (i.e., RNAScope) to confirm the down regulation of *Cacna1g* mRNA, leading to the suppression of CaV3.1. The Covid-19 pandemic significantly delayed the work, and my collaborator did not mark the mice that received scramble control and *Cacna1g* shRNA viruses. Therefore, we do not have comparable results for whether CaV3.1 is knocked down.

Introduction

Animal activities such as exploring the surroundings, escaping from predators or dangers, or searching for food rely on locomotion. The neural commands for movement initiation and termination have been implicated to originate in different supraspinal brain regions. In all cases, motor commands must be processed by the basal ganglia and enacted by the reticular activating system (RAS) of the lower brainstem (Groenewegen, 2003). The series of connections from the basal ganglia to the brainstem are essential in eliciting voluntary motor movements in animals. Hierarchically, the sequence of locomotor activation takes the following path: motor commands enter the striatum (most likely from neocortex), which is the input layer of the basal ganglia, and projects to the substantia nigra pars reticula (SNpr), the principal output nucleus of the basal ganglia. Striatal and SNpr neurons are both inhibitory (GABAergic) and both exert inhibitory control over several motor areas in the brainstem, which in turn control the central pattern generators for basic motor functions such as eye-head orientation, locomotion, mouth movements, and vocalization (Hikosaka, 2007). The motor command then goes from SNpr to the mesencephalic locomotor region (MLR) in the upper brainstem. The MLR is hypothesized to integrate numerous sensorimotor, cognitive, and limbic inputs to regulate locomotion directly, through descending pathways to spinal locomotor networks (Noga et al., 2003, 2017; Ryczko & Dubuc, 2013), and indirectly through ascending connections to other higher brain centers (Kroeger et al., 2017; Martinez-Gonzalez et al., 2012). The MLR then projects to the RAS of the lower brainstem, which is glutamatergic like the MLR. Descending commands from the RAS go to central pattern generator microcircuits in the spinal cord.

In the MLR exists pedunculopontine nucleus (PPN), a locomotor-related site located in the mesencephalic and upper pontine tegmentum. The PPN receives inputs from, but does not

project equally strongly back to, the SNpr; also, the PPN projects to the RAS. Due to its widespread connections to other areas of the brain and spinal cord, the PPN is involved in a wide range of physiological and behavioral processes, including locomotion, gait control, and regulation of rapid eye movement sleep and wakefulness (Martinez-Gonzalez et al., 2012). Growing evidence suggests its clinical relevance as a potential target for treating motor symptoms associated with Parkinson's disease (PD). The deep brain stimulation (DBS) of the PPN has been proposed and proven in initial stages to improve gait and fall disorders in patients with PD (Lin et al. 2020). Therefore, investigating the function of PPN neurons at the cellular and ion channel levels, as well as its synaptic activation mechanisms, could be applicable for the treatment and prevention of PD and other neurodegenerative diseases.

Another region that has caught the neuroscientists' attention is the cuneiform nucleus (CnF), a nucleus dorsal to the PPN, also a key part of the MLR. Neuronal circuits in PPN and CnF both contribute to the maintenance and speed of locomotion while only CnF is able to elicit high-speed synchronous locomotor activity. On the other hand, PPN neurons project more broadly to neurons in the pons and medulla, which CnF neurons do not project to, therefore may provide descending pathways for slow forms of locomotion pertaining to exploration and quotidian tasks (Caggiano et al., 2018). Through combining kinematic analysis and electrophysiological recordings, another study exhibits that the glutamatergic CnF neurons initiate locomotion and accelerate locomotor rhythm, thus giving rise to running gaits. PPN, in contrast, contributes to slow-walking gaits and regular locomotor, which corresponds to daily tasks except perhaps reserved for emergencies like escaping a predator; CnF appears to be more important for those emergent locomotor tasks (Josset et al., 2018). Additionally, the PPN

receives direct input from the SNpr as the afferent gamma aminobutyric acid (GABA) endings from SNpr synapse with PPN cell bodies and dendrites (Granata and Kitai, 1991).

This thesis focuses on the influence of glutamatergic PPN neurons on RAS neurons and thus the central pattern generators (CPG) in the spinal cord. The previously mentioned circuit involving the basal ganglia and the brainstem includes inhibitory relationships, which are the postsynaptic connections by the striatum and SNpr, as well as excitatory relationships, which are the postsynaptic connections by the MLR and RAS. The key question is: how does the brain initiate a movement and how does it do so?

According to the longstanding – but untested – *disinhibition hypothesis*, in the basal ganglia, the striatum and the SNpr have a disynaptic disinhibition relationship (Grillner, 2006). The striatum at rest is silent, its neurons remain in a so-called "Down" state wherein the membrane potential remains hyperpolarized below -70mV, and thus have no influence in the SNpr because they are not active. In contrast, SNpr neurons spike tonically as their default state (DeLong and Georgopoulos, 1981). Therefore, we posit that when the striatum is at default resting state, the SNpr exerts tonic GABAergic inhibitory effect on the PPN. Since the PPN is inhibited at rest by default, it is unable to activate the RAS, inhibiting arousal and limb movements, and thus locomotion. On the other hand, when the striatum receives cortical input, it actively inhibits the SNpr, which will in turn disinhibit the PPN. Disinhibited PPN neurons exert glutamatergic effect on the RAS and in turn the CPG to generate locomotion. We will explore the cellular and ion channel mechanisms by which disinhibition evokes motor commands.

In current literature, the PPN has been proven to directly influence the CPG and hence the nucleus's effects on rhythmic outputs of the limbs. However, it is the disinhibition relationship between the SNpr neurons and PPN neurons that has not been explicitly proven.

Therefore, I will perform multiplex *in situ* hybridization to investigate how excitatory PPN neurons respond to disinhibition. We posit that PPN neuronal release from SNpr inhibition evokes a low-threshold Ca^{2+} spike (LTS), which is only possible if the neuron starts from the hyperpolarized membrane potential such as would occur if it were tonically inhibited by default (as is the case in the SNpr → PPN synaptic microcircuit). At a hyperpolarized membrane potential, low-threshold Ca^{2+} channels are de-inactivated. When the membrane rebounds from hyperpolarization, it activates the Ca^{2+} current to thus generate an LTS. In other words, voltage-gated Ca^{2+} channels are activated and produce an LTS, which is kinetically slower than conventional Na^{+} bursting spikes, thus a burst of conventional Na^{+} spikes may ride atop the LTS.

In PPN neurons, we have evidence that *Cacna1g* gene, which encodes the CaV3.1 proteins, make up the low-threshold Ca^{2+} channels that we argue are evoked during disinhibition and which mediate the LTS burst responses that we posit cause downstream postsynaptic activation of the RAS and ultimately the CPG in the spinal cord. By injecting a specially designed short hairpin RNA (shRNA) virus, a custom-designed RNA probe used to silence target gene expression via RNA interference (Moore et al., 2010), my team can target and downregulate the translation of *Cacna1g* to CaV3.1 proteins. If the disinhibition hypothesis is correct, and our specific hypothesis that low-threshold Ca^{2+} currents mediate the motor command from the MLR to RAS, then attenuating the expression of low-threshold Ca^{2+} channels will reduce the burst responses mediated by the low-threshold Ca^{2+} current. Preventing bursts, we contend, will "short circuit" the system and thus disable locomotion despite a sensory input to the striatum and a functional circuit.

In this thesis, I will perform post-injection histology to verify that the shRNA was accurately injected into the PPN and that CaV3.1 proteins are downregulated. Via *in situ*

hybridization analysis, I will be able to confirm the down regulation of *Cacna1g* mRNA. Though the Covid-19 pandemic significantly delayed the project, I was still able to assess CaV3.1 knockdown, allowing the project to continue.

Materials and Methods

Mice

We used transgenic VGlut2-Cre$^{(+/+)}$ (8-20 weeks old) mice that have Cre recombinase expression in excitatory glutamatergic cells. Animal care and handling were performed according to the guidelines of the Institutional Animal Care and Use Committee (IACUC) at the College of William & Mary. Mice were 12 weeks old when injected and only females were used in the 2-week interval (injection to tissue processing) group.

shRNA-Containing Viral Vectors

We used a gene expression vector containing *Cacna1g* shRNA and the reporter protein mCherry. The shRNA construct consists of specific shRNA target sequences in the *Cacna1g* gene (NCBI 12291, RefSeq NM_001112813.2) to knockdown the gene expression of CaV3.1 ion channel was packaged together into an adeno-associated virus serotype 9 (AAV9) delivery vector. The AAV9 also carries a gene to express fluorophore mCherry, which was used to locate the area of expression that was targeted using viral vector delivery method through stereotaxic injection. Control experiments utilized a similarly designed shRNA except that the same set of nucleotides were scrambled such that the resulting sequence did not target any known gene, and certainly not *Cacna1g*.

Robotic Stereotaxic Injection

Virus injections were performed in deeply anesthetized 12-week-old female mice, placed in a motorized, computer-controlled stereotaxic frame (Neurostar Robot Stereotaxic). Anesthesia was induced with 2.5% isofluorane throughout the entire injection. Bilateral craniotomies 4.5-4.7 mm posterior to the bregma point and 1.2-1.3 mm later to the midline were performed. Each side was loaded 100nL of AAV using Neuros Syringe (Hamilton Company, Reno, Nevada). Viral

vector was injected at a rate of less than 75nl/min for a period of 10 minutes. Fluorescent signals of mCherry expression verified the proper viral injections of both the experimental and scramble injections.

Tissue processing

Two weeks post-injection (Px) mice were anesthetized using 0.1mL Beuthanasia per 10g of the animal's body weight. The animals were perfused (transcardially) with 4% paraformaldehyde (PFA) in 10X PBS at pH 7.4. The tissue was postfixed in PFA overnight at 4^{o}C and transferred to 1X PBS after 24 hours until ready for sectioning protocol. Midbrain MLR region was sectioned in alternating thickness of 30 µm for *in situ* hybridization and 50 µm for mCherry expression confirmation. 30 µm sections were stored in 0.5X TBS + 0.1% Tween 20 (TBST) at 4^{o}C until ready for *in situ* hybridization protocols. 50 µm sections with the addition of DAPI dye to stain the nucleus were viewed under the fluorescent microscope to confirm the expression and location of mCherry.

In Situ Hybridization

In situ hybridization was carried out according to ACD Bio's (Advanced Cell Diagnostics, Newark, CA) RNAscope Multiplex Fluorescent v2 assay using radiolabeled oligonucleotide probes designed to bind to specific target RNA and detectable in one of 3 fluorescent channels, Channel 1 (C1), Channel 2 (C2), and Channel 3 (C3). The experimental probes used were *Cacna1g* for C1 and mCherry for C3 and were visualized using fluorophores Opal 520 and Opal 690 (Akoya Biosciences, Menlo Park, CA), respectively. A negative control probe, which did not contain *Cacna1g* and mCherry, was also used for all animals. Sections were first washed with TBST and mounted onto Superfrost Plus (Fisher Scientific, Waltham, MA) slides to dry at room temperature for 1 hour. The sections were washed in water and dried at

room temperature for another 1 hour before being baked at 60°C for 1 hour. The sections were postfixed at 4°C for 1 hour using 4% PFA in 10X PBS. The sections were then dehydrated using an ethanol gradient of 50%, 75%, and 100%. The sections were left to dry at 60°C for 15 minutes then were added hydrogen peroxide to sit for 10 minutes. The sections were rinsed with water and dried at 60°C for 15 minutes. Target retrieval (1X) reagent, which contains citric acid and lithium dodecyl sulphate, was used to boil the sections at about 100°C for 10 minutes. The slides were then dehydrated with 100% ethanol and dried at 60°C for 10 minutes before they were left to incubate overnight at room temperature.

The RNAscope Assay is proceeded by adding protease to catalyze the hydrolysis of proteins for 30 minutes at 40°C. Fluorophores (Opal 520 and 690) were prepared in TSA buffer using ratio of 1 to 1500. The sections were incubated for 2 hours at 40°C after the C1/C3 probes were added to the sections. Sections were then rinsed twice (2 minutes each) in 1X wash buffer. The signal amplification was carried out by adding ACD Bio RNAscope's Amp1 and repeated for two more times using Amp 2 and 3. After each hybridization, the sections were baked for 30 minutes at 40°C and washed twice in 1X wash buffer. Next, fluorophores are incorporated. Signal development is carried out with HRP-C1, which is used for channel 1. Sections were baked for 15 minutes at 40°C and washed twice in 1X wash buffer. Opal 520 was then added to the sections to incubate for 30 minutes at 40°C. After washing twice in 1X wash buffer, HRP blocker was added. The sections were baked for another 15 minutes at 40°C before washing in 1X wash buffer to conclude C1 fluorophore dyeing. The same procedure was carried out for C3 but this time using Opal 690. Sections were counterstained with DAPI, cover-slipped using Prolong Gold Antifade Mountant (Thermo Fisher Scientific, Waltham, MA) and kept overnight in the dark.

Two-photon imaging

We imaged the mCherry, DAPI, and *Cacna1g* expression in the PPN in sections obtained from 6 mice using a multi-photon laser-scanning microscope (Thorlabs, Newton, NJ). We collected images of the whole section using 10x magnification with 512x512 pixels and of the PPN using 40x magnification with 1024x1024 pixels. We used scanning sequence beginning with 642nm, then 488nm, and finally 405nm wavelengths for mCherry, *Cacna1g*, and DAPI detection, respectively. Power, gain, and digital offset, a setting used to subtract background noise to optimize contrast, were set to maximize distinct fluorescence without bleeding through, over-saturating, and bleaching. Bleed-through occurs when multi-color microscopy improperly assigns probe species, which affects the reliability of information and quantification of the species.

Image Analysis

The high magnification 40x magnification images were analyzed using QuPath software to localize mCherry expressing cells and *Cacna1g* transcripts within these mCherry expressing cells. QuPath is a bioimage software that is an open-source solution for whole slide image analysis (Bankhead et al., 2017).

Images were inserted and "fluorescence" was selected for image type. Brightness and contrast were adjusted for *Cacna1g* transcript expression to maximize visibility. mCherry infected cells were identified using "cell detection." Minimum area, maximum area, and threshold were adjusted depending on the fluorescence of the mCherry expressing cells. Over-segmentation (counting multiple cells instead of one cell) and false positives were minimized by adjusting background radius and sigma. After identifying all mCherry expressing cells, "subcellular spot detection" was selected to localize *Cacna1g* transcripts in mCherry expressing

cells. Detection threshold, expected spot size, minimum spot size, and maximum spot size were adjusted to accurately detect *Cacna1g* transcript "dots."

Data were extracted from QuPath into Microsoft Excel to compile the average number of transcripts per mCherry expressing cells for each of the 6 animals.

Results

Viral vector delivery into the PPN cells

To target glutamatergic neurons in the PPN, we used injections of Cre-dependent adeno-associated virus stereotype 9 (AAV9) carrying mCherry and *Cacna1g* shRNA or scramble shRNA. Both the *Cacna1g* shRNA and scramble injected mice treated with experimental probes *Cacna1g* and mCherry during *in situ* hybridization expressed mCherry proteins in infected cells in the PPN region and the surrounding regions (Figures 1A-F). To confirm that viral vector delivery was injected into the PPN, we utilized a 40x magnification to confirm mCherry expression (642nm) in the PPN neurons of all 6 animals that received the experimental probes (Figures 2A-F). From Figures 2A-F, we can see that not all cells were infected with the AAV9. Some animals exhibited higher infection rates (Figure 2D) while some exhibited lower infection rates (Figure 2E). This was not due to the different parameters of confocal imaging but to the nature of the infection rates. From the 40x confocal image sequence, we included *Cacna1g* (488nm) detection as well (Figures 3A-F). When zoomed in closely into the images for image analysis, we saw individual puncta, which are individual bright spots that are different from circular regions of fluorescence. We were able to conclude that one punctum was one *Cacna1g* transcript because of the theory behind RNAScope. The experimental probes treated cells have fluorophores scaffolding surrounding mCherry proteins and *Cacna1g* transcripts, making these molecules fluoresce under confocal microscopy. Therefore, bright puncta were, in fact, *Cacna1g* transcripts with thick scaffolding of the probe, thus exhibiting a strong signal. Larger fluorescing regions that were not puncta were not *Cacna1g* transcripts but were due to the nature of the 488nm wavelength, which is a naturally occurring fluorescence that absorbs more than other wavelengths.

Colocalization of channels

To confirm the colocalization of DAPI, mCherry expressing cells, and *Cacna1g* expressing cells, we zoomed into the 40x magnification of the PPN of Vu06-2 (Figures 4A-C). Consistent throughout the results, the red pseudocolor is mCherry proteins, the blue pseudocolor is DAPI, and the green pseudocolor is *Cacna1g* transcripts. In Figure 4A, we showed 2 channels: mCherry and DAPI. DAPI stained all cells while mCherry proteins are only present in AAV9 infected cells. In this figure, we can confirm that not all cells were infected by AAV9. In Figure 4B, DAPI and *Cacna1g* channels are shown. Here, we see that *Cacna1g* transcripts were even less populated than compared to mCherry proteins from Figure 4A. This could be due to a few reasons. The first reason would be that individual puncta are hard to visualize at a low magnification. DAPI fluorescence may also be masking some puncta. Furthermore, unlike mCherry proteins, *Cacna1g* transcripts are mRNAs that are significantly smaller molecules compared to proteins, meaning decreased surface area for the scaffolding to attach to, in turn having smaller areas of fluorescence. Lastly, mRNAs are generally fewer in number than proteins in cells due to the nature of translation, where one mRNA could be translated multiple times by ribosomes before being degraded. Thus, *Cacna1g* transcripts have inherently less visible signal both due to size and number. In Figure 4C, all 3 channels are presented. *Cacna1g* transcripts appear both inside and outside mCherry expressing cells because all PPN cells have the *Cacna1g* gene. However, our focus is only the *Cacna1g* transcripts in the mCherry expressing cells as these cells are the ones that were injected either with the *Cacna1g* shRNA or scramble AAV9. Limiting quantification to mCherry expressing cells allows us to compare the effect of gene knockdown by *Cacna1g* shRNA to cells that received the scramble virus.

Figure 5 shows a more zoomed in version of the PPN at 40x magnification of the same animal Vu06-2. This figure exhibits all 3 channels and pinpoints cells that display variations of channels. The white arrow shows a cell that colocalizes all 3 channels, meaning the cell was successfully infected by AAV9 and also expresses *Cacna1g* transcripts. The yellow arrow shows a cell that expresses both DAPI and mCherry but does not express transcripts. This could be due to the insufficient amount of the mRNA to be successfully tagged by probes during RNAScope. The green arrow shows a cell that was not infected by the AAV9 but nonetheless expresses *Cacna1g* transcripts. This could happen as the *Cacna1g* gene is present in all PPN cells described previously.

QuPath cell detection and subcellular spot detection

In order to quantify *Cacna1g* transcripts in mCherry expressing cells, we utilized the QuPath software. QuPath allows the function of cell detection, where we adjusted the parameters to detect individual mCherry expressing cells (Figures 6A-B). Figure 6A is zoomed in to the PPN at 40x magnification of animal Vu06-3. Individual puncta can be seen both inside and outside the mCherry expressing cells. After applying the appropriate parameters, puncta inside the mCherry cells were identified and counted (Figure 6B). The QuPath software allows for precise detection of these puncta as we could set the minimum and maximum sizes of subcellular spot detection to prevent counting large, circular signals in previous figures. Moreover, only those puncta with high enough signal intensity were detected as transcripts.

Quantification results from QuPath are presented in Table 1. The table shows the number of mCherry expressing cells detected (column 2), number of *Cacna1g* transcripts detected (column 3), and the average number of *Cacna1g* transcripts in each mCherry expressing cell (column 4). In all animals, there was fewer than one transcript per cell. We were unable to

compare the experimental group and the scramble group due to my collaborator not noting the animals that received the experimental *Cacna1g* shRNA virus or control scramble shRNA virus.

Negative control probe

To verify that the probes' attachment to experimental probes were not random, we also included negative probe treatment to all animals. In Figure 7A-F, we imaged the PPN at 40x magnification of cells that were treated with the negative probe, which did not contain mCherry and *Cacna1g*. This means that although there were mCherry proteins and *Cacna1g* present in these cells, they were not tagged by the probe to display the signals during confocal imaging. However, since all cells (both experimental probes treated and negative probes treated) were stained by DAPI at the end of the RNAScope, negative probes treated cells still exhibit DAPI fluorescence. In Figures 7A-F, the same sequence of confocal imaging to the experimental probes treated cells was applied, and no signals other than DAPI were detected. Therefore, we can conclude that the experimental probes treated cells did not exhibit mCherry and *Cacna1g* fluorescence arbitrarily.

Discussion

The goal of this thesis was to confirm that the shRNA was accurately injected into the PPN and that CaV3.1 proteins were downregulated. Through multiplex *in situ* hybridization (i.e., RNAScope), I automated the detection of *Cacna1g* mRNA and showed amount of this transcript following shRNA knockdown.

Two-Photon Imaging

Our confocal imaging of the whole section and of the PPN at 10x and 40x robustly showed 3 channel expressions (DAPI, mCherry, and *Cacna1g*) with high clarity. At each magnification, cells were identified clearly by applying relatively consistent parameters throughout the imaging process. Images produced in this project were also realistic as it showed different cells expressing either or both mCherry proteins and *Cacna1g* transcripts. This is normal as we have evidence that all PPN cells have CaV3.1 proteins, meaning experimental probe treated cells that were not infected by the AAV9 could still display strong *Cacna1g* signals. Clear images like the ones produced in this project are essential in RNAScope quantification and the study of gene knockdown in general as this topic requires high precision and accuracy. Through this thesis, we demonstrated that we are qualified and skilled to conduct gene knockdown studies as we could produce high precision and clarity images that are essential to the project.

Some caveats we experienced during confocal imaging include the speed of sections being bleached due to the nature of RNAScope analysis reagents. This was especially the case for DAPI imaging which required high intensity. We would recommend minimal exposure to DAPI wavelength (405nm) when setting parameters prior to imaging to prevent bleaching desired regions in the future. Furthermore, we could have reduced the background noise of the

experimental probes treated cells by subtracting the negative probe treated cells had we used the same parameters for imaging the two groups.

Image Analysis

QuPath software successfully automated cell detection and subcellular spot detection in all animals. This was a significant breakthrough for the lab as we had manually counted transcripts in the past. By using QuPath for quantification, significant time and energy were saved. Future analysis could greatly benefit from standardization of parameters during imaging and quantification to provide reliable and consistent data.

Though many of the features ImageJ offers are offered by QuPath, we still utilized the ImageJ software for some functions to optimize analysis speed and ease. For example, ImageJ was used to assign pseudocolors, adjust contrast and brightness, and set the scale bar. However, QuPath was chosen over ImageJ because ImageJ was unable to produce satisfactory cell and transcript analysis. When attempting to quantify individual mCherry expressing cells, ImageJ counted empty spaces as cells, as it did not have the appropriate threshold function for our purposes. During cell detection analysis in QuPath, we optimized the parameters to produce the most accurate cell and subcellular transcript detections. However, in trying to optimize the results, some false positives and misses were produced. Therefore, we increased the sigma value, which smoothened or decreased segmentation for cell detection, in the cell detection parameter. In other words, cells that were supposed to be singular but were marked as multiple cells were corrected to a singular cell. By increasing sigma, we ensured that over-segmentation did not occur, but it sometimes resulted in larger cells going undetected as well. To remove false positives and separate densely packed nuclei in clusters, we decreased the background radius in the cell detection parameter. One caveat of removing false positives by decreasing the

background radius was that some cells were not counted. Therefore, we were very careful in choosing the appropriate background radius to ensure all visually inspected cells were counted in QuPath. Another challenge we experienced was the value of the threshold. Due to the nature of different signal intensities of mCherry expressing cells, some cells were low in intensity and were not detected by the program while other noises were detected. To ensure that noises would not be detected, the negative control probe treated images could be subtracted from the experimental probes treated images. This way, we could decrease the intensity of the threshold and detect all cells without picking up background noise.

Subcellular spot detection also required careful maneuvering of parameters. When some transcripts were undetected, we decreased the minimum spot size or detection threshold. However, false positives would appear due to the decreased size and lowered threshold. To counter this issue, we persisted with the detection threshold that accurately distinguished non-transcript from transcripts and decreased the minimum spot size so that some cells may pick up false positives to compensate for missed spots in other cells. As some images included bright regions of *Cacna1g* transcripts, we were unable to determine whether these regions also included puncta that should be counted because the entire region had a very strong fluorescence signal. However, those cases were rare and were easily fixed by adjusting the power and gain during two-photon microscopy imaging.

In future studies, we recommend making sure exposure time was uniform for experimental and negative control of one animal to subtract potential noise, which could decrease false positives and misses. We also recommend seeking extensive training from the ACD technician group for more specific inquiries regarding this set of RNScope analysis.

Ideally, incorporating a manual selection after automation in QuPath would greatly enhance future cell detection and subcellular spot detection analyses.

Data Analysis

We were able to quantify data from all six animals using relatively uniform procedure thanks to the QuPath software. mCherry expressing cells and *Cacna1g* transcripts expressed in those cells were quantified automatically and the average number of transcripts per cell were easily calculated. However, we experienced a significant setback during data analysis as my colleague did not understand the nature of a double-blind study. Therefore, when performing stereotaxic injections in the animals, my colleague did not note which animals received the scramble virus or the *Cacna1g* shRNA. As a result, we were not able to analyze the differences between the experimental and control groups.

Despite this setback, we did not expect CaV3.1 knockdown to be statistically significant at the 2 weeks injection point. Instead, we hypothesized that CaV3.1 knockdown will be more apparent in longer injection points, such as 4 weeks and 6 weeks, that will be conducted.

Conclusion

The goal of this thesis was partially fulfilled as we were able to verify the correct injection of the virus into the PPN. However, we were unable to verify the down regulation of CaV3.1 in *Cacna1g* shRNA virus due to the mistake mentioned previously. On a brighter note, automation for quantification was a success that could greatly benefit the lab in future RNAScope studies.

Due to the Covid-19 pandemic, this project was significantly delayed. We intended to include data from multiple injection points, not just from the 2 weeks interval. However, this

project established a strong foundation for the continuation of this study as I was able to solidify the RNAScope procedure and the image analysis for future experiments.

Next steps

The immediate next step in this research will be to repeat this study as no valid data was produced for the 2 weeks time interval. Next, the period between injection and dissection will be extended to study the long-term effect of the shRNA virus on the PPN. The lab plans to inject groups based on three different time intervals: 2 weeks (14 days), 4 weeks (28 days), and 6 weeks (42 days). The same procedures will be conducted similarly to the steps listed above with modifications to address relevant issues. Histology will be performed to confirm injection into the PPN and *in situ* hybridization will be performed to quantify the level of *Cacna1g* transcripts to compare the effect of differential time interval on the rate and amount of CaV3.1 gene knockdown in glutamatergic neurons of the PPN.

After successfully knocking down CaV3.1 proteins and optimizing the injection time period, the next project will be to study the electrophysiology of glutamatergic neurons in the PPN that contain CaV3.1 proteins. To confirm the hypothesis that low threshold Ca^{2+} channels are, in fact, responsible for locomotion, behavioral tests will be conducted before and after viral vector delivery. However, it is also essential to take into account the downstream pathway – PPN's activation of RAS before the signal excites the CPG. Ultimately, elucidating the signal transduction and neuron properties of the circuit described have great potential in understanding neurodegenerative diseases and other physiological responses to stimuli that have been extensively studied.

References

Bankhead, P., Loughrey, M. B., Fernández, J. A., Dombrowski, Y., McArt, D. G., Dunne, P. D., McQuaid, S., Gray, R. T., Murray, L. J., Coleman, H. G., James, J. A., Salto-Tellez, M., & Hamilton, P. W. (2017). QuPath: Open source software for digital pathology image analysis. *Scientific Reports*, *7*(1), 16878. https://doi.org/10.1038/s41598-017-17204-5

Caggiano, V., Leiras, R., Goñi-Erro, H., Masini, D., Bellardita, C., Bouvier, J., Caldeira, V., Fisone, G., & Kiehn, O. (2018). Midbrain circuits that set locomotor speed and gait selection. *Nature*, *553*(7689), 455–460. https://doi.org/10.1038/nature25448

Delong, M.R. and Georgopoulos, A.P. (1981) Motor functions of the basal ganglia. In: Brooks V.B. (Ed.), The Nervous System. American Physiological Society, Bethesda, MD, pp. 1017-1061.

Granata AR, Kitai ST. Inhibitory substantia nigra inputs to the pedunculopontine neurons. Exp Brain Res. 1991;86(3):459-66. doi: 10.1007/BF00230520. PMID: 1761086.

Grillner, S. (2006). Biological Pattern Generation: The Cellular and Computational Logic of Networks in Motion. *Neuron*, *52*(5), 751–766. https://doi.org/10.1016/j.neuron.2006.11.008

Groenewegen, H. J. (2003). The basal ganglia and motor control. *Neural Plasticity*, *10*(1–2), 107–120. https://doi.org/10.1155/NP.2003.107

Hikosaka, O. (2007). GABAergic output of the basal ganglia. *Progress in Brain Research*, *160*, 209–226. https://doi.org/10.1016/S0079-6123(06)60012-5

Josset, N., Roussel, M., Lemieux, M., Lafrance-Zoubga, D., Rastqar, A., & Bretzner, F. (2018).

Distinct Contributions of Mesencephalic Locomotor Region Nuclei to Locomotor Control in the Freely Behaving Mouse. *Current Biology*, *28*(6), 884-901.e3. https://doi.org/10.1016/j.cub.2018.02.007

Kroeger, D., Ferrari, L. L., Petit, G., Mahoney, C. E., Fuller, P. M., Arrigoni, E., & Scammell, T. E.

(2017). Cholinergic, Glutamatergic, and GABAergic Neurons of the Pedunculopontine Tegmental Nucleus Have Distinct Effects on Sleep/Wake Behavior in Mice. *The Journal of Neuroscience: The Official Journal of the Society for Neuroscience*, *37*(5), 1352–1366. https://doi.org/10.1523/JNEUROSCI.1405-16.2016

Lin F, Wu D, Lin C, Cai H, Chen L, Cai G, Ye Q, Cai G. Pedunculopontine Nucleus Deep Brain Stimulation Improves Gait Disorder in Parkinson's Disease: A Systematic Review and Meta-analysis. Neurochem Res. 2020 Apr;45(4):709-719. doi: 10.1007/s11064-020-02962-y. Epub 2020 Jan 16. PMID: 31950450.

Martinez-Gonzalez, C., Wang, H.-L., Micklem, B. R., Bolam, J. P., & Mena-Segovia, J. (2012). Subpopulations of cholinergic, GABAergic and glutamatergic neurons in the pedunculopontine nucleus contain calcium-binding proteins and are heterogeneously distributed: Subpopulations of neurons in the PPN. *European Journal of Neuroscience*, *35*(5), 723–734. https://doi.org/10.1111/j.1460-9568.2012.08002.x

Moore, C. B., Guthrie, E. H., Huang, M. T.-H., & Taxman, D. J. (2010). Short Hairpin RNA (shRNA): Design, Delivery, and Assessment of Gene Knockdown. *Methods in Molecular Biology (Clifton, N.J.)*, *629*, 141–158. https://doi.org/10.1007/978-1-60761-657-3_10

Noga, B. R., Kriellaars, D. J., Brownstone, R. M., & Jordan, L. M. (2003). Mechanism for

activation of locomotor centers in the spinal cord by stimulation of the mesencephalic locomotor region. *Journal of Neurophysiology*, *90*(3), 1464–1478. https://doi.org/10.1152/jn.00034.2003

Ryczko, D., & Dubuc, R. (2013). The multifunctional mesencephalic locomotor region. *Current Pharmaceutical Design*, *19*(24), 4448–4470.

Figure 1. *mCherry and Cacna1g expressions in 10x magnification*

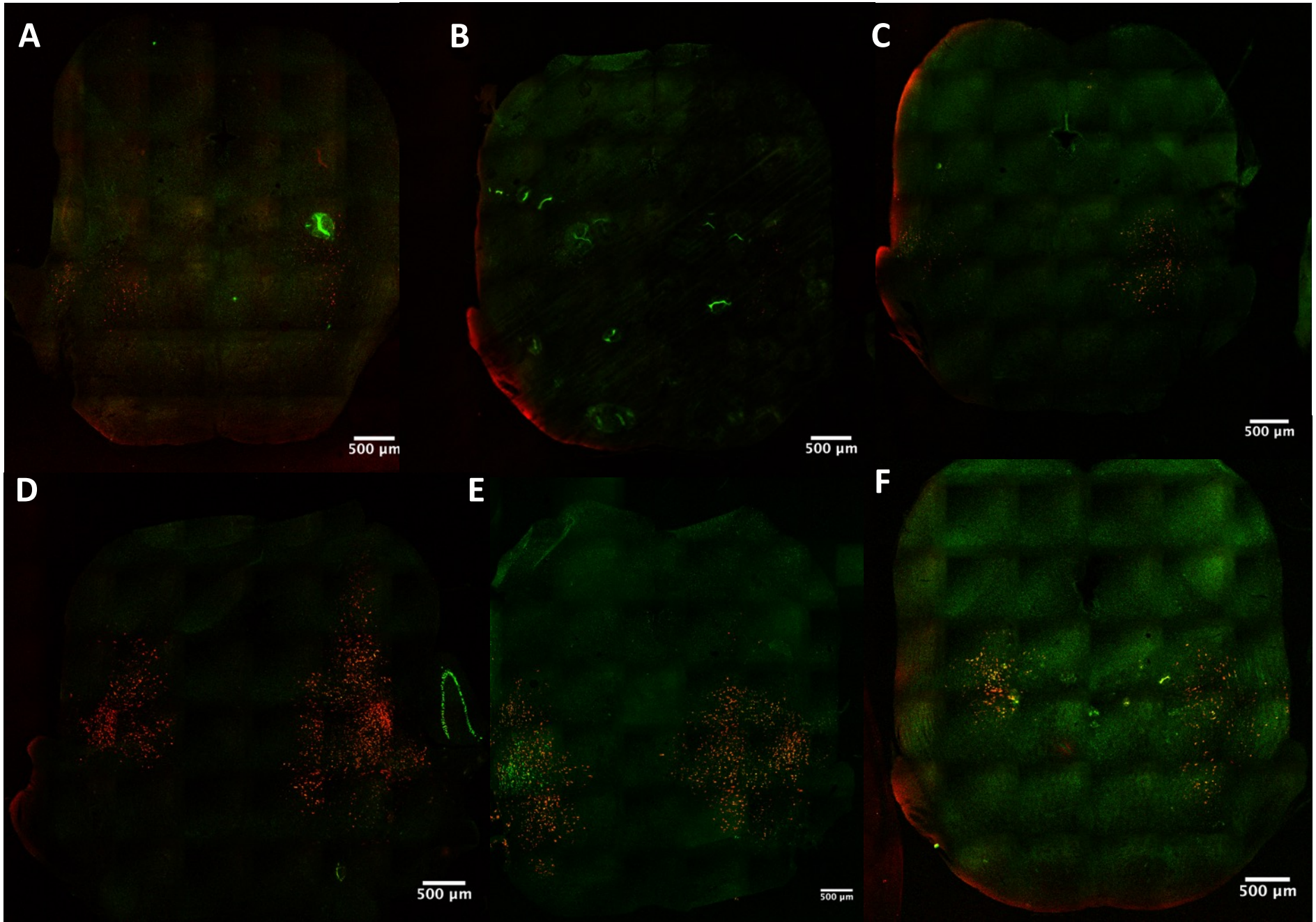

Figures 1A-F show the 10x magnification horizontal section of the PPN in Vu04-1, Vu04-2, Vu06-1, Vu06-2, Vu06-3, and Vu06-4 mice, respectively. Red pseudocolor corresponds to mCherry protein expression and green pseudocolor corresponds to *Cacna1g* expression. The low magnification view shows the regions of bilateral injection into the PPN. mCherry is expressed in all sections as all viral vectors contained the mCherry sequence. *Cacna1g* were expressed in scramble groups ___ as scramble shRNA did not knockdown CaV3.1. Figure 1A shows mCherry expression in bilaterally, verifying injection into the PPN. mCherry expression was relatively low in Figure 1B due to unprecise injection. Figure 1C shows more mCherry expression on the right, suggesting an off-target injection on the left. Figure 1D shows mCherry expression bilaterally, with larger area of expression on the right. Figure 1E and 1F show mCherry expression bilaterally.

Figure 2. *mCherry expression in 6 animals at 40x magnification*

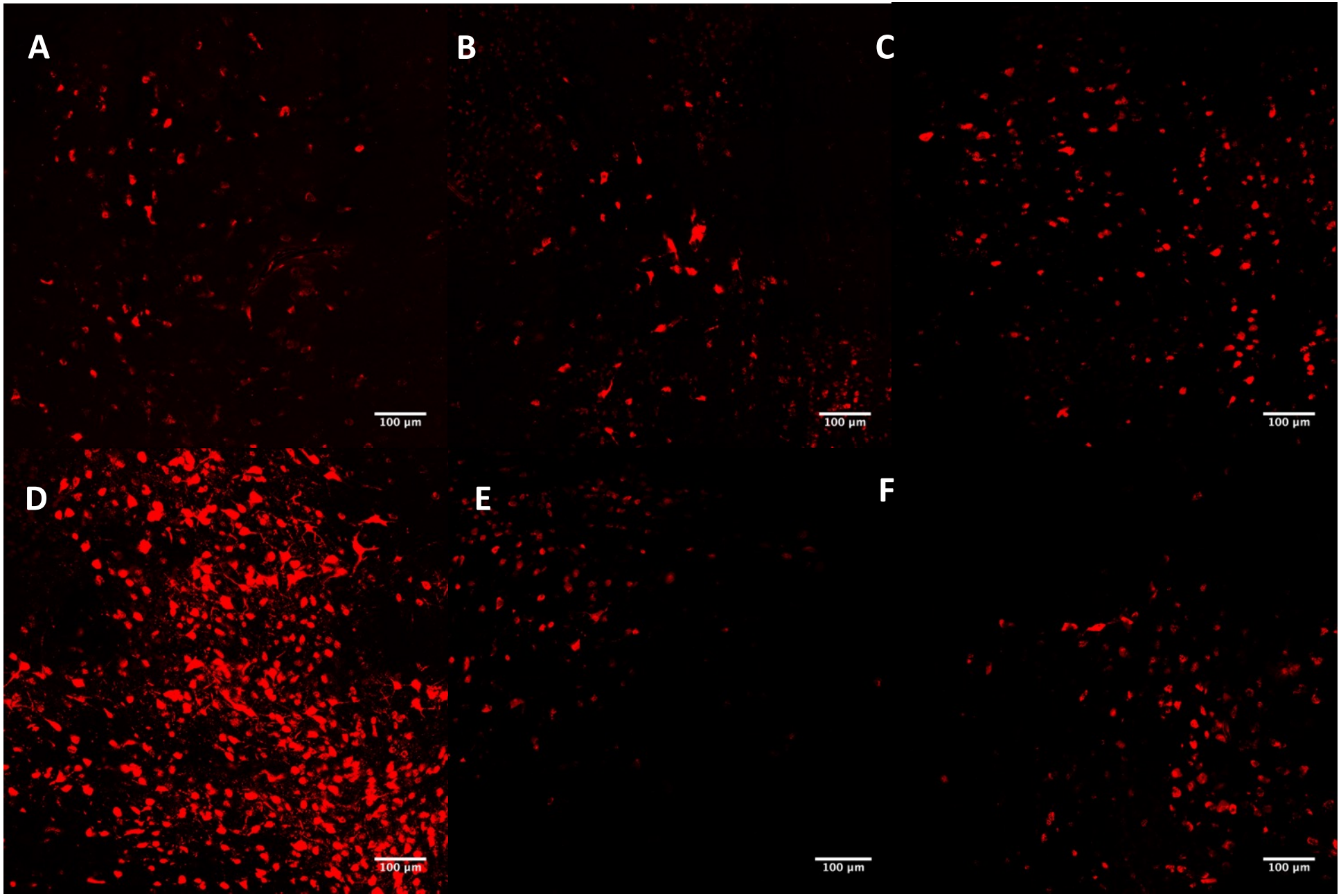

Figures 2A-F show the 40x magnification of the PPN expressing mCherry proteins in Vu04-1, Vu04-2, Vu06-1, Vu06-2, Vu06-3, and Vu06-4 mice, respectively. All sections are of the left PPN other than Vu06-3 and Vu06-4. The side with more distinct expression was imaged.

Figure 3. *Cacna1g expression in 6 animals at 40x magnification*

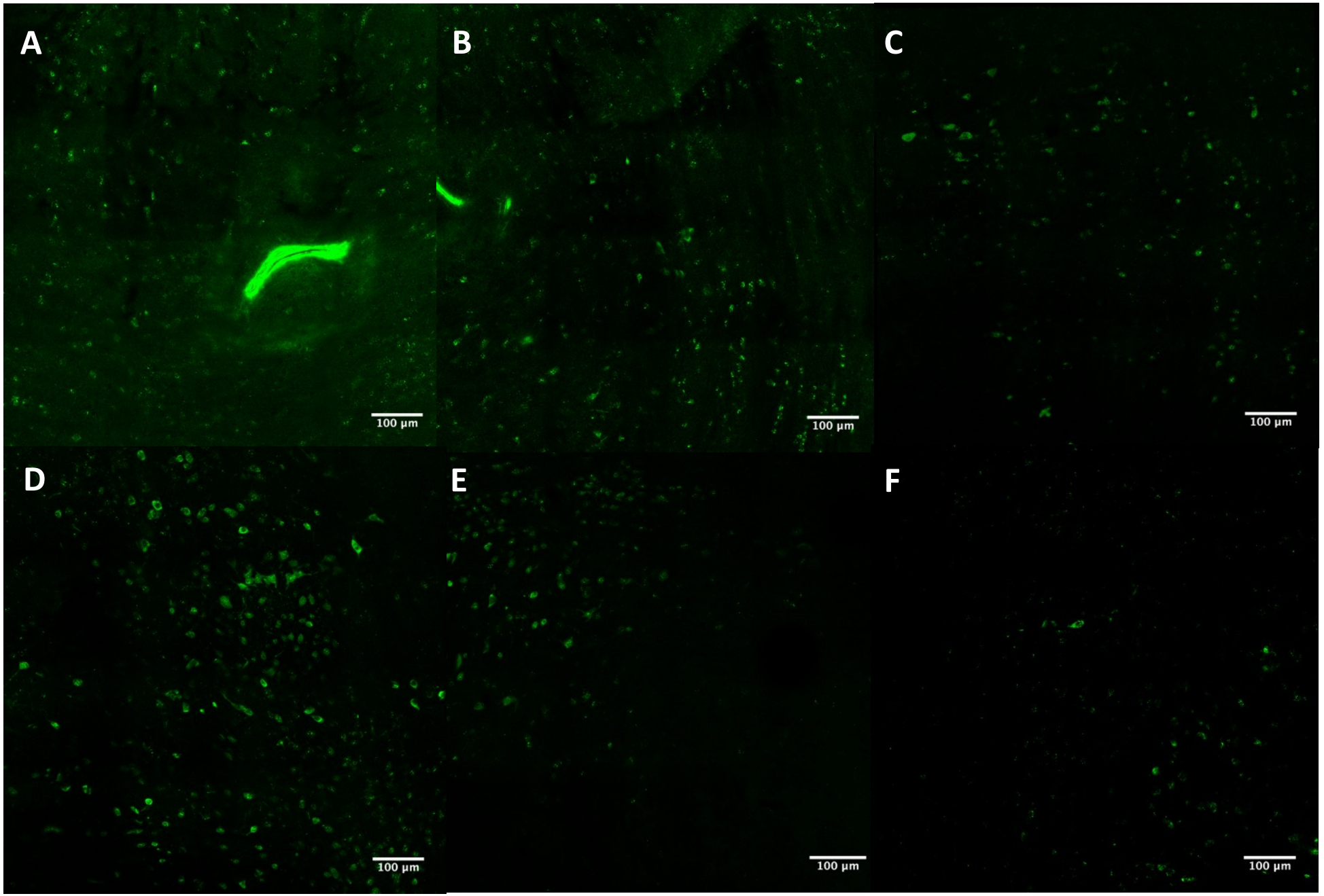

Figures 3A-F show the 40x magnification of the PPN expressing *Cacna1g* transcripts in Vu04-1, Vu04-2, Vu06-1, Vu06-2, Vu06-3, and Vu06-4 mice, respectively. All sections are of the left PPN other than Vu06-3 and Vu06-4. The side with more distinct expression was imaged.

Figure 4. *Colocalization of DAPI and mCherry expressing cells, DAPI and Cacna1g expressing cells, and all 3 channels expressing cells all at 40x magnification of Vu06-2*

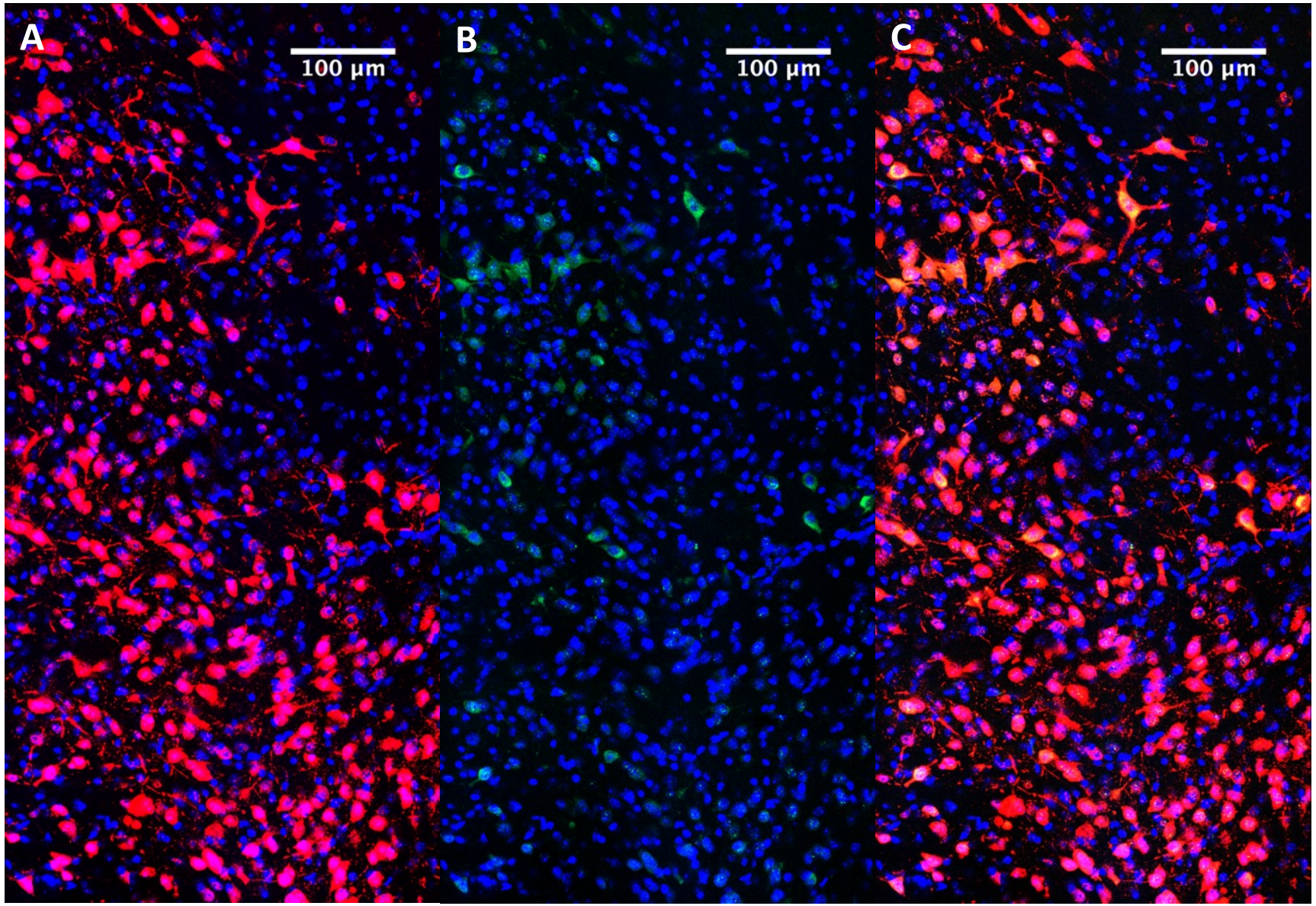

Figures 4A-C show the same region of Vu06-2. Figure 4A shows DAPI (blue) and mCherry (red) expressing cells. All cells express DAPI fluorescence. Only those successfully received the viral vector express mCherry proteins. Figure 4B shows all cells and *Cacna1g* transcript (green) expressions. *Cacna1g* transcripts are potentially present in all cells. However, we are interested in transcript expression only in mCherry expressing cells as mCherry confirms viral delivery into cells. Figure 4C shows all 3 expressions.

Figure 5. *Zoomed in 40x magnification of cells expressing DAPI, mCherry, and Cacna1g cells (white arrow); DAPI, mCherry, but no Cacna1g cells (yellow arrow); and DAPI, no mCherry, Cacna1g cells (green arrow) of Vu06-2*

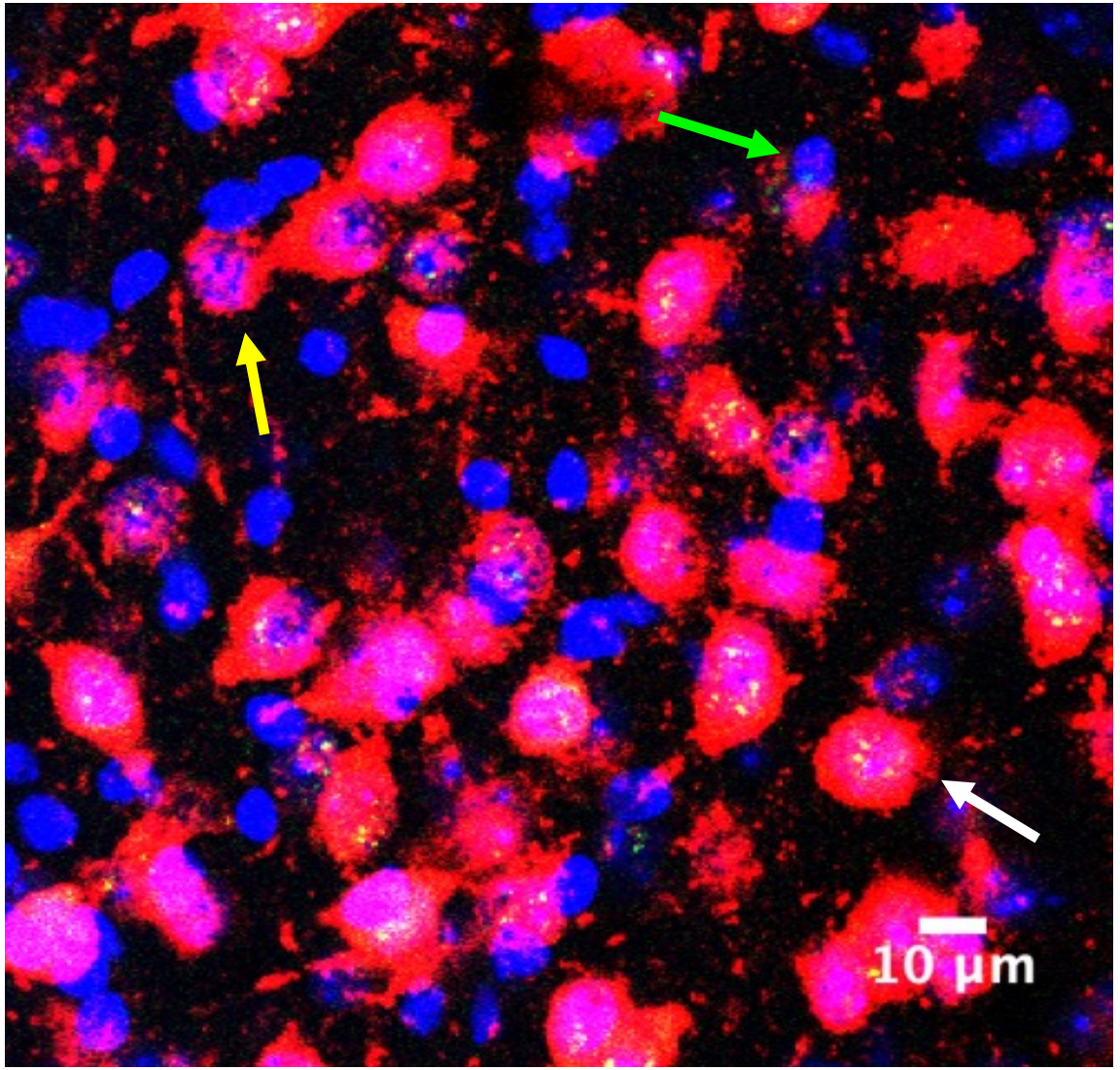

Figure 5 shows a zoomed in section of Vu06-2 that shows expression of DAPI (blue), mCherry (red), and *Cacna1g* transcripts (green). The white arrow shows a cell that expresses all 3 channels. The yellow arrow shows a cell where DAPI and mCherry co-express but without *Cacna1g* transcripts. The green arrow shows a DAPI expressing cell that isn't infected as it does not express mCherry proteins but nonetheless express *Cacna1g* transcripts. For the purpose of this study, only transcripts expressed in mCherry expressing cells are quantified as mCherry expression confirms viral vector delivery.

Figure 6. *QuPath cell detection and subcellular spot detection of mCherry and Cacna1g expressions of Vu06-3*

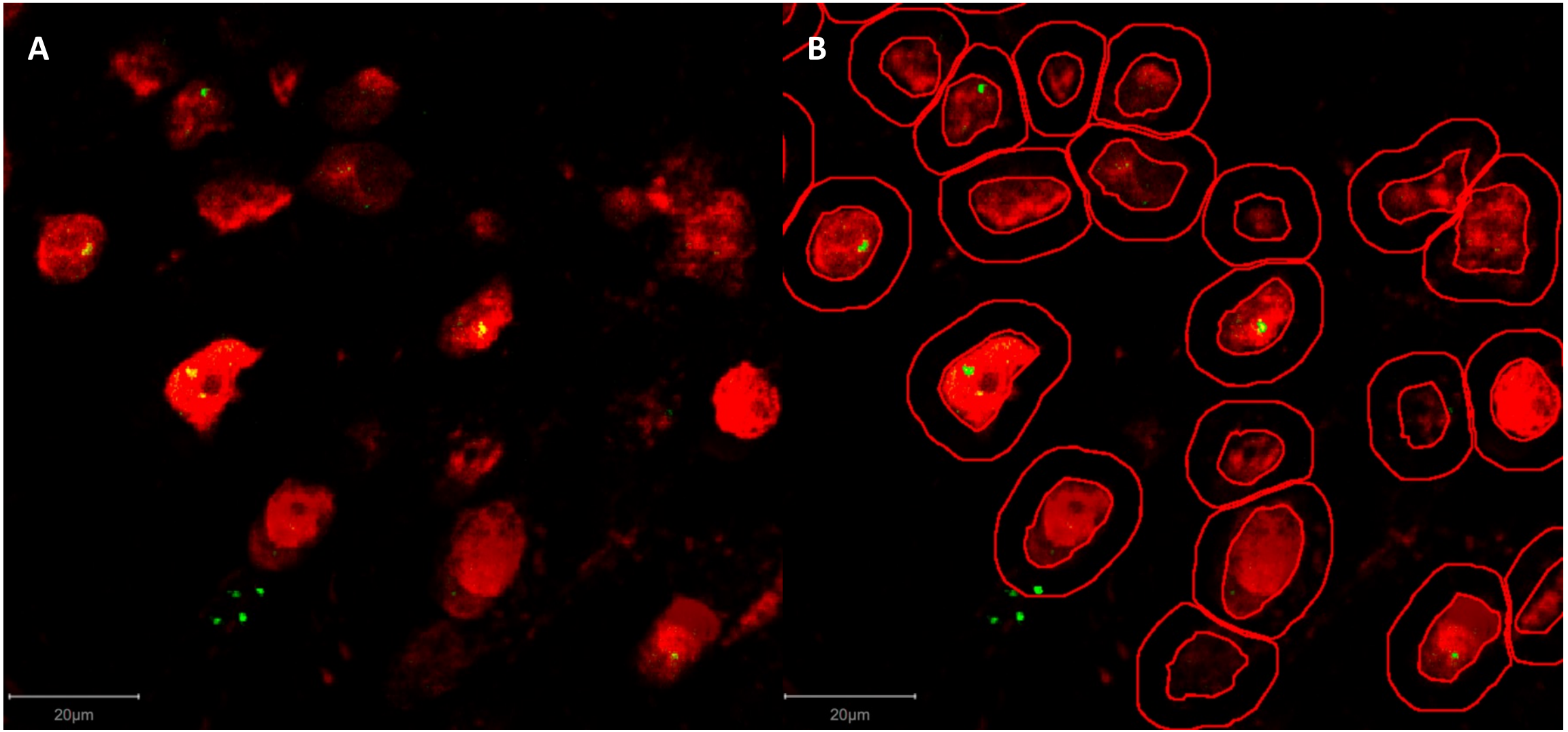

Figure 6A shows a zoomed in region of the PPN of Vu06-3 that expresses mCherry and *Cacna1g* transcripts in the QuPath program. Figure 6B shows cell detection in red lines and subcellular transcript detection in green lines. The inner line represents nucleus detection, and the outer line represents the cell wall. Transcripts outside mCherry expressing cells were not counted.

***Figure** 7. Negative control expressing DAPI, mCherry, and Cacna1g in 6 animals at 40x magnification*

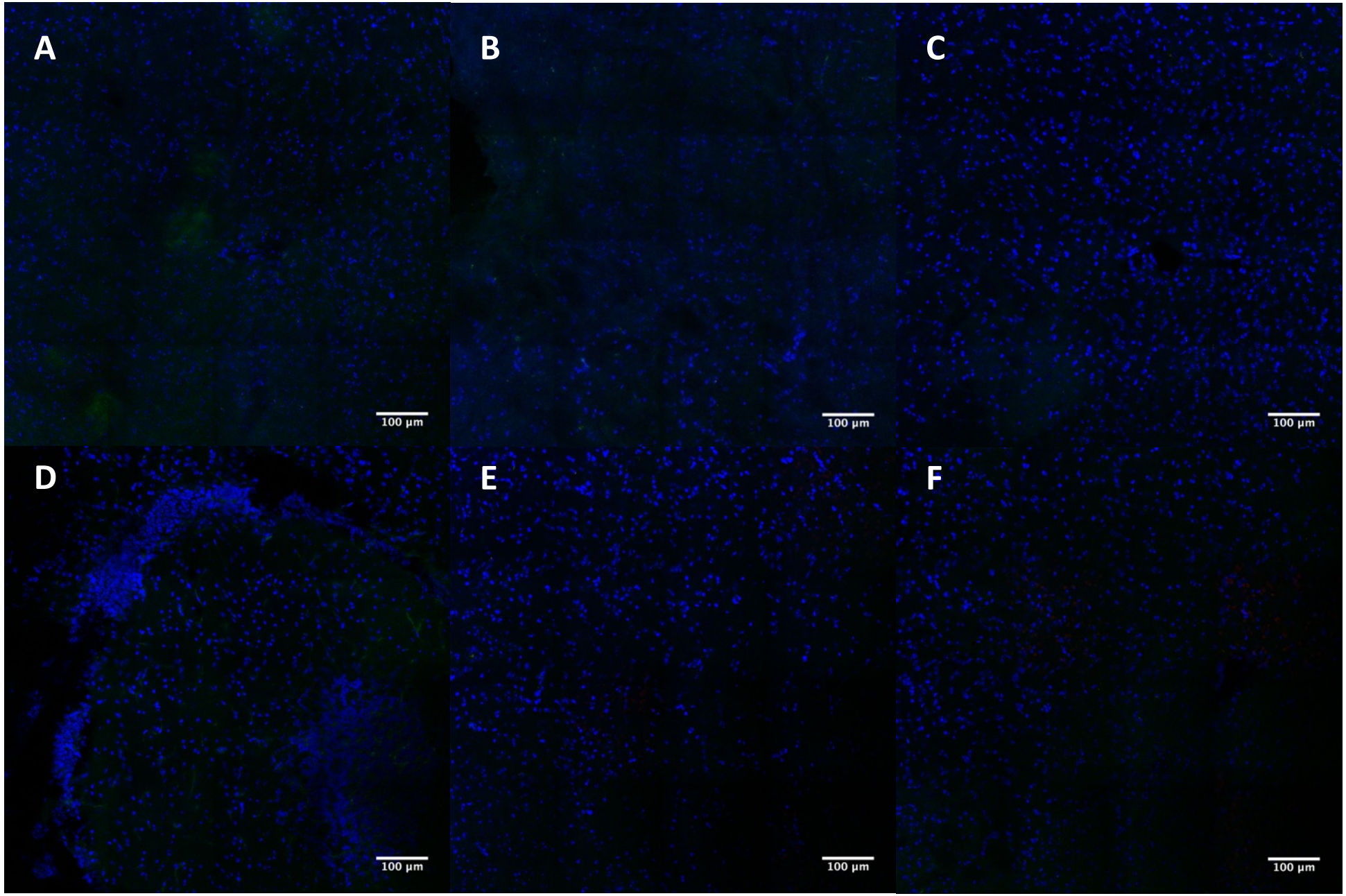

Figures 7A-F show the 40x magnification of the PPN using negative control probe during *in situ* hybridization for Vu04-1, Vu04-2, Vu06-1, Vu06-2, Vu06-3, and Vu06-4 mice, respectively. As negative control probes do not contain mCherry and *Cacna1g* tags, none of the negative control sections express fluorescence under the same settings as experimental probe group.

***Table 1**: average number of Cacna1g transcripts detected in mCherry expressing cells*

	Number of cells detected	Number of transcripts detected	Average number of transcript/cell
Vu04-1	45	25	0.555555556
Vu04-2	27	10	0.37037037
Vu06-1	157	45	0.286624204
Vu06-2	634	173	0.272870662
Vu06-3	179	52	0.290502793
Vu06-4	113	77	0.681415929

Table 1 shows the numerical quantification from QuPath. The average number of *Cacna1g* transcripts in mCherry expressing cells were calculated by dividing number of cells detected (column 3) by number of transcripts detected (column 2).

Table 1 shows the numerical quantification from QuPath. The average number of *Cacna1g* transcripts in mCherry expressing cells were calculated by dividing number of cells detected (column 3) by number of transcripts detected (column 2).